STUDIES INTO SYNERGETIC EFFICIENCY OF DRIVEN VERTICAL AXIS PROPELLERS

By

Tanner Blackledge Penrod, B.S.

A Project Submitted in Partial Fulfillment of the Requirements

for the Degree of

MASTER OF SCIENCE

in

Mechanical Engineering

University of Alaska Anchorage

August 2020

APPROVED:

Jifeng Peng, Ph.D., Committee Chair
Jennifer Brock, Ph.D., Committee Member
Getu Hailu, Ph.D., Committee Member

Getu Hailu, Ph.D., Chair
Graduate Mechanical Engineering Department
Jennifer Brock, Ph.D., Associate Dean
College of Engineering

Abstract

In the quickly expanding field of Industrial Multirotor Drones, one of the main limitations is flight time of current multirotor systems. A method of increasing the flight time is to improve the efficiency of the aircraft design. One possibility for increasing efficiency is synergetic design. Synergetic design is a principal where two or more systems are designed to interact to increase the efficiency of the complete system. In the wind turbine industry, synergetic spacing has been used for increasing the efficiency of vertical axis wind turbines by utilizing staggering. Staggered horizontal axis wind farms have been shown to increase the efficiency by as much as 5% over aligned. These methods even more effective for vertical axis wind turbines due to their specific wake pattern. This project reports the results of synergetic efficiencies of driven propellers in various configurations utilizing a test stand. The design requirements for this stand included minimizing outside interference, the ability to test a wide variety of propellers, and have a built-in measurement system for the required calculations. The measurements that were required included the power consumption, rotational speed, thrust output, and spacing of the motors. The test stand also features a custom electronic system for running the systems. The objectives that were completed by the electrical system included driving the motors, setting the desired speed, and measuring the rotations per minute. Data collection methods and raw data gathered are described, discussed, and compared to theoretical maximum efficiency of the propulsion system.

Table of Contents

List of Figures

Page

List of Appendices

Page

Introduction

The drone industry has seen a tremendous amount of growth since the FAA introduced Part 107 commercial drone operations in 2016 [1]. The part 107 licensing program is a system that simplified the process of obtaining a commercial drone license in the United States. The industrial growth has affected a variety of different fields including agriculture, construction, and mining [1]. The industry is expected to grow from $4.4 billion in 2018 to $63.6 billion by 2025 [1]. One of the biggest limitations to the industry is flight time of multirotor aircraft [2]. This limitation is currently blamed on the low power density of batteries, when compared to fossil fuel sources [2]. One of the possible solutions to this is using a different power source [2]. A possible option that is currently being looked at is using hydrogen fuel cell powered drone systems [1]. Fuel cell powered systems have three times the flight time of a comparable battery solution [1]. Fuel cell powered systems are not without their issues though. The first of these issues is sourcing the hydrogen [1]. Ballard Unmanned Aerial Systems, a company that is developing fuel cell powered drones, claims it can take a few weeks to get gas cylinders and safety equipment to certain locations [1]. Another common industry method to increase flight time of multi-rotor style drones is the use of hybrid power systems with an internal combustion engine running a generator [1]. These systems can offer longer range but can be less reliable compared to options like fuel cells [1].

A possible solution to increasing the flight time is to design a multirotor system using synergetic design principals. One study into synergetic design looked at using synergetic design in the wind turbine industry [3]. In horizontal axis wind turbines, staggering their position can increase the efficiency by up to 5% [3]. The efficiency gains can be even higher for vertical axis wind turbines due to their unique wake [3]. This wake is caused by the turbines' omnidirectional design [3]. The efficiency gains of well-designed clusters of vertical axis wind turbines can be as much as 10% per turbine [3]. Additional spatial efficiency can be gained due to there being up to three times the number of turbines in each area of land [3].

Another field that has done research into the effect of propeller spacing on efficiency is high altitude range solar-powered unmanned aircraft [4]. These high-altitude aircraft fly in low Reynolds number environmental regime [4]. In this region of the atmosphere there are dramatic reductions in the propulsive and aerodynamic efficiencies due to thin air [4]. This aerodynamic regime leads to the use of

large aspect ratio wings with distributed multi propeller propulsion systems [4]. These aircraft have more of a design challenge due to magnified effects in these flight regimes [4]. One area that has a major effect is the design of the propulsion system [4]. For instance, higher speed propellers are preferred due to the higher speed reducing the swirling effects on the wing [4]. This leads to the use of a higher number of smaller propellers rather than the larger, slower propellers in other high efficiency aircraft design [4]. In the findings from this research there were advantages to propellers at closer spacing [4]. One advantage was the reduction of the tip vortices due to the mutual counteraction of the propellers at closer spacing [4]. Another advantage was the more continuous pressure sub-regions over the airfoil [4]. This reduces the induced drag caused by the change in pressure over the span wise pressure gradients [4]. Testing showed an eighteen percent decrease in drag from using the closer, optimized propeller spacing [4]. This reduction in drag did come at a cost of an increased propeller disk loading, which reduces the motor efficiency [4].

Test Stand Design

There were several design parameters for the test stand frame. The first task was the thrust from both motors needed to be measurable with one force sensor. The motors also had to be attached in a way allowing them to be adjusted to permit testing at different propeller spacing settings. These parameters were accomplished by using a rail system. The rail system was built out of 8020 brand aluminum profile to allow for a simple-to-construct and modular system that allows components to be easily changed as testing required. In order to measure the force from both motors with one force sensor, the sensor was mounted to the center of the rail system and the motors were spaced symmetrically on the rail system. To space the motors symmetrically, rulers centered at zero were used on both sides of the rail.

Below the rail system is a larger frame which serves multiple purposes. The first purpose was to provide a fixed point to mount the force sensor. The frame was fixed into place by clamping it to a pair of workbenches. These workbenches were at least 50 times the weight of the maximum thrust expected, and so the test stand base was assumed to be fixed. The outer frame was also used to mount the test stand between two workbenches, which raised the motors above ground effect. Another purpose of the

lower frame was for mounting the electrical components of the test stand. All the electrical components that needed to be mounted were designed with 8020 T-nut mounting points to allow them to be attached to the frame. The final advantage of the lower frame was to provide a boundary during testing. The complete test stand assembly can be seen in Figure 1.

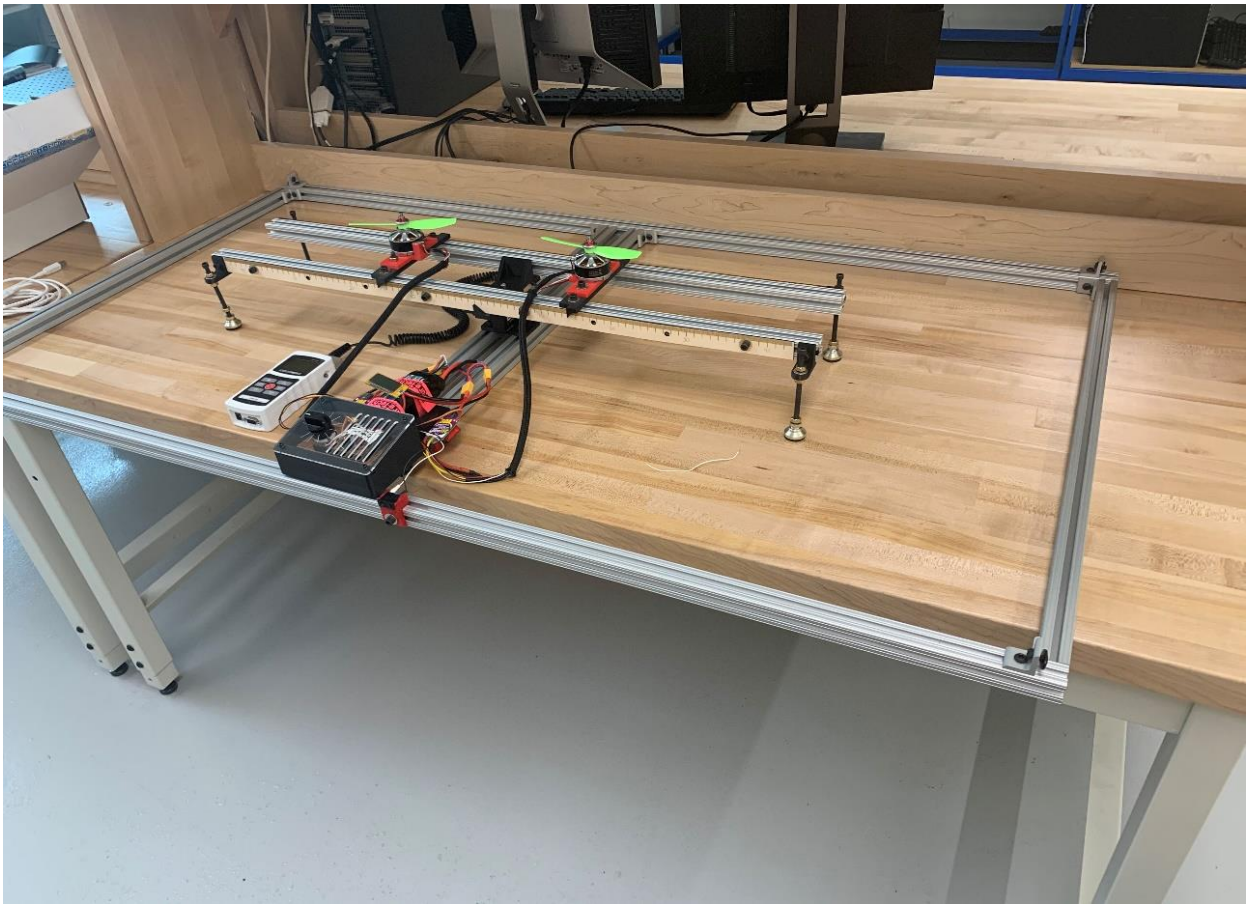

Figure 1: Test stand setup for dual motor tests

Midway through testing, the researcher thought the center mount for the mark 10 force sensor might be causing interference with the flow. This was due to the propellers overlapping the center mount during some of the testing of the smallest spacing increments. This caused the downstream flow region conditions to change with the spacing. This change adds inconsistency with the flow which in theory could cause issues with the data due to changing ground effect scenarios. To check this theory, a set of blocks

was created to raise the motors above the rails. Each block raised the motor by one inch, and a maximum of three blocks could be used with the longest bolts available in the size used for the motor mounts.

Electronic Design

The electrical system on the test stand serves multiple purposes. The first purpose is to run the motors at a constant setting. This system needed to work at a wide range of speed settings and needed to produce repeatable results. Another requirement was data collection. The required measurements included the lift of the motors, the power output of the battery, and the speed of the two motors. The original test stand electronics used a constant revolutions-per-minute (rpm) system with a built-in current sensor to make the measurements during the test cycle. The constant rpm system worked on a Proportional-Integral-Derivative (PID) loop, measuring the rpm and adjusting as required to bring the rpm to the desired setting [5]. The lift was measured using an external force sensor. The force sensor used was a Mark 10 MR03-10, the data sheet for this sensor can be found in Appendix A. The measurements from this sensor would be manually measured and added to the results from the built-in sensors.

The original test stand electronics failed during the early testing, thus requiring a new system. The biggest correction from the lessons learned was changing from a constant rpm to a constant power setting system. The reason for this change was to remove the requirement for a PID loop. PID loops need to be tuned when conditions change [5], which the researcher worried might affect the results of this test. In a PID loop there is typically a steady state error of around five percent, which the system will try to correct for with minor changes [5], so avoiding a PID system was expected to lead to a more stable equilibrium. The constant power setting system used the standard servo pulse width modulation settings in the electronic speed control to set the motors to a certain percentage of full power. This percentage of full power leads to a constant power output for a given test, giving it a more stable steady state. In this system, the rpm of the motors would still be measured, but the rpm would not be a defining variable. The decision was made to switch to all manual measurements from gauge-style outputs rather than automatic data logging, so that measurements could all be taken once the system reached an apparent equilibrium. The external measurements added to the original system were the power output (in watts) and the rpm of

each motor. And the final design change was adding a safety switch that could disable the motors at any time during the test.

The physical layout of the electrical circuit can be separated into several categories. The first type of circuit layout used in the system was an Arduino compatible switch. This was used for each pin on the rotary switch and the safety switch for a total of eleven copies. This circuit used was the standard circuit

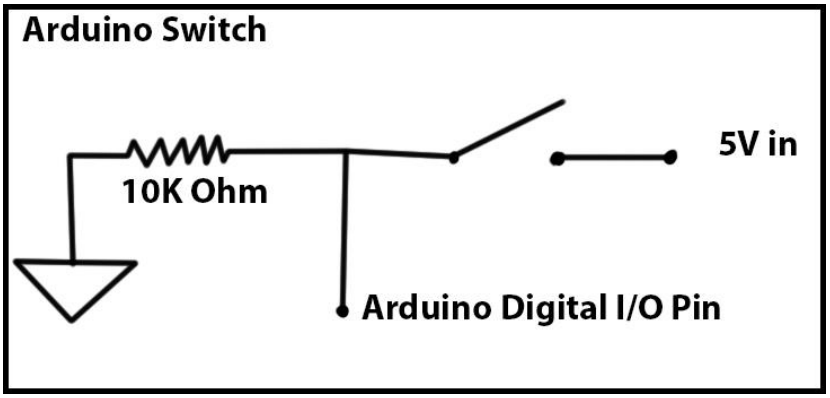

Figure 2: Diagram of the standard circuit used for a switch

for an Arduino button with a pull-down resistor [6]. An individual switch circuit diagram can be seen in Figure 2. The next category of circuit is the electronic speed control controller. This system was only used

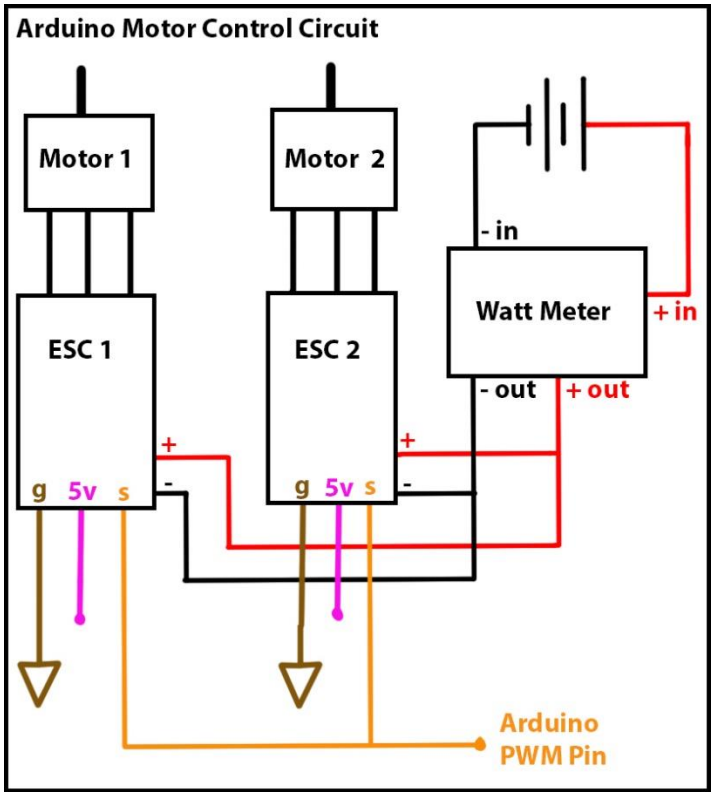

Figure 3: Motor Control Circuit

once on the electrical system. This circuit is a modified version of the Arduino servo control circuit [7]. It was modified by disconnecting the positive wire from the electronic speed controls. This was due to the electronic speed controls having five-volt outputs instead of five-volt input on a servo. The circuit diagram for this sub section can be seen in Figure 3. And the final category of circuit used in the test stand's circuit was the rpm sensor circuit. This section is used to hook up the US1881 latching Hall effect sensors to the Arduino to be used to read the rpm of the motors. The specific information on the US1881 Hall effect can be found in the spec sheet in appendix A. The three pins on the sensor were hooked up so that the signal pin is connected to a pulse width modulation capable Arduino pin with the ground and five-volt pins being

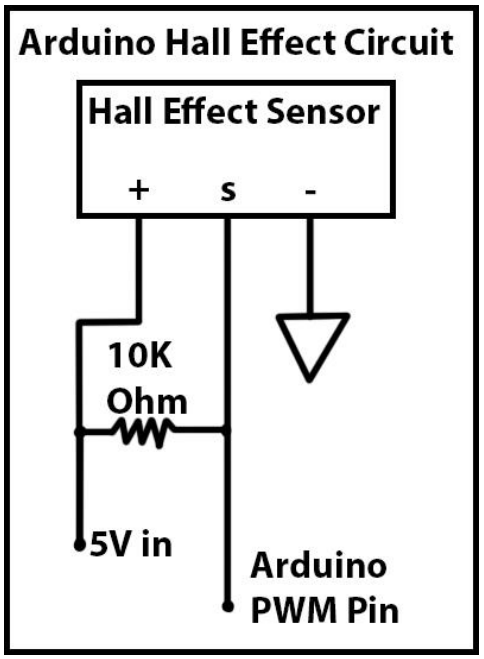

Figure 4: Hall Effect Sensor Circuit

hooked up to those respective locations on the Arduino. There was an additional 10k ohm resistor between the positive and signal pin to bring the signal voltage up to five-volts [8]. This circuit diagram can be seen in Figure 4. All these sections make up the circuit, of which the diagram can be seen in Appendix B.

Arduino Code

The Arduino code for running the test stand can be separated into two sections: the code for running the motors, and the code for measuring the motor rotations per minute. See Appendix C for the complete code for the test stand. This code was based on a few example sets of code in order to ensure

that the code would work with existing libraries. The first example code was the “button” Arduino, which was used for the different switches [6]. The next example is the servo microsecond, for the esc programming [9]. And the final example code used was the timer1 used to create the timer used for measuring the rpm [10].

The first of the two major parts of the code for running the motors is including the “Servo.h” library. This library contains a set of functions needed to control a servo or other device using the radio control pulse width modulation [7]. The electronic speed controllers used for the motors use this type of pulse width modulation. The next section needed for the motor control was the pin setup on lines 8 through 19. Line 8 sets “esc1” to a servo variable, which was used for controlling both electronic speed controllers. Lines 9 through 19 set the pins for the different switches for the system. S1 was for the shutoff switch and r2 through r11 were for the rotary switch contacts. The pins for the switches were chosen to simplify the circuit layout. The next section required for running the motors is the first part of the void setup on lines 60 through 73. Line 60 attached the electronic speed control servo pin to pin 5 which is a pulse width modulation capable pin on the Arduino Mega. Line 61 set the initial servo setting to 1000 microseconds which is equivalent to idle for an electronic speed controller using standard servo pulse width modulation. The next part that pertains to the motors is a void loop starting on line 82. This section starts by creating state variables for each of the switch poles except the two off position pins. Each of these state variables is looking for the state or digital reading of each of the pins used for the switches. The next part of the loop was the series of “if” and “else if” statements used to determine the speed setting. Each of these statements is looking for a high, or on, signal from both the safety switch and one of the speed setting pins on the rotary switch. If both conditions are met the Arduino will send the signal to the electronic speed controls to set the motor power output to the desired value. If both of those conditions were not met, then the code falls back to the “else” statement which shuts down the motors. Using the else statement to disable the motors is a safety feature of the test stand. This is because the motors will default to an off position if an unforeseen error causes an input other than one of the planned inputs.

The second part of the code is used for measuring the rpm of the two motors. This part of the code starts with the including the “TimerOne.h” library. This library was used to create a simplified method to use the pulse width modulation pins to measure the frequency of an interruption signal [10]. The next part of the code used for the motor speed measurement is lines 5 and 6 which were used to set the interrupt pins for the two hall-effect sensor signal pins. The pins were set to pins 2 and 3 on the Arduino. The next section for measuring the motor speed is from lines 21 to line 57. The first part of this section created two integer values used for two counting values for the motor speed measurement on lines 22 and 23. Line 26 created a floating variable for the number of motor magnetic poles. This set the number of hall-effect magnetic pulses per rotation of the motor. Lines 30 through 40 setup an interrupt service routine, ISR, counter for each of two motor rpm sensors. On lines 43 through 57 are the timer functions for the two rpm sensors, the code for both sensors is identical and will only be explained once. The timer process was as follows: first stopping the timer, calculating the rpm of the specific motor, displaying the value on the serial monitor, and finally resetting the counter value. The equation for calculating the rpm was the number of pulses divided by the number of poles multiplied by 60 seconds. The 60 seconds is due to the timer period being one second, this is set later in the code on line 75. This process is in a loop which repeats for the timer period of 1 second. And the final sections of the code pertaining to the motor speed measurement system are on line 62 and lines 75 through 78 in the void setup section. Line 62 sets the baud rate for the serial port to 57600 bits per second, which was the limit of the port on the computer used for the testing. As mentioned before line 75 sets the period for the timer. Lines 76 and 77 attach the variables used for each motor to the correct timer. These also set the counting variable as a rising counter in order to have the system count up rather than down from a number. And to finish of this section of the code line 78 attached the ISR counter variables from the section starting on line 43 to the timer. And this concludes the code for the test stand, thus concluding all aspects of the test stand design.

Preparing Test Stand

The process of data collection was as follows. First, the motors were checked to confirm the power was disabled by unplugging the main battery from the y-harness. The propellers desired for testing were then installed onto the motors. Once installed, the propeller nut, nut A in Figure 5, torque was checked by confirming that the propeller could not be spun by hand when the motor was held. After the propellers were installed, the motor spacing was set to the desired width and the mounting bolts, C in Figure 5, were tightened to prevent the motors from sliding on the rails. The motor mounts were confirmed to be perpendicular to the rails by checking that the measurements on both the front and back of the test stand rulers are equal. This was done to ensure that the motor spacing measurements were

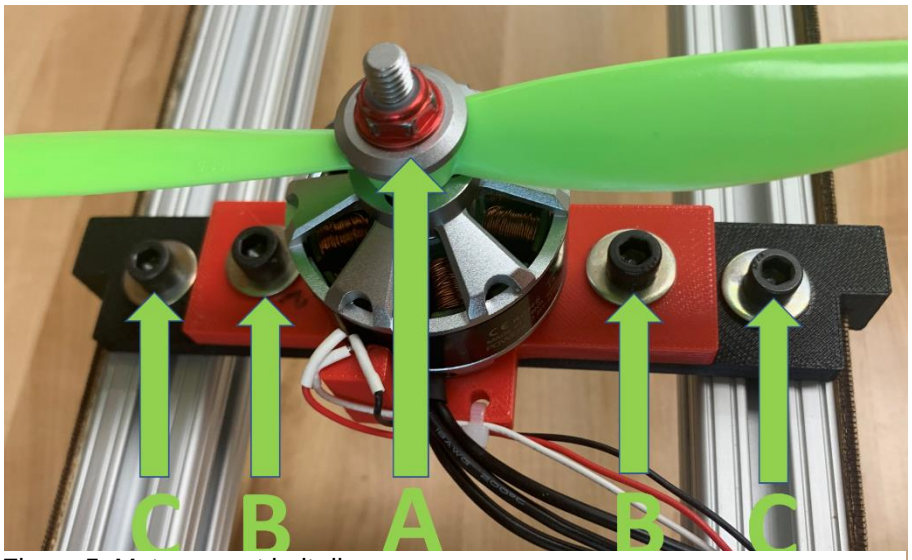

Figure 5: Motor mount bolt diagram

accurate. Once the spacing was set and both propellers were installed, the propellers were freely spun to ensure that the propellers did not contact each other. This was done because the motors are not synchronized which prevents testing when the propellers are intermeshed. Once the clearance was checked, the test stand was ready for a motor check. The Arduino's USB cord was plugged into the computer running the Arduino software and the serial monitor was opened. Before plugging in the main battery to the y-harness, the controls were checked that the speed selection dial was set to zero and the safety switch was set to "off". With all objects and persons clear of the internal area of the test stand, the main battery was plugged into the y-harness in order to start the motor arming process. Once the ESCs emitted a standard set of beeps, the arming process was complete, and the motors were ready to run. To

test the motors before testing, the safety switch was turned on and the dial was set to the first notch, the motors would run at the slowest speed set in the firmware. Both motors were checked to ensure that they were producing positive thrust. If either of the motors were spinning the incorrect direction, then any two of the three motor power wires, the three large black wires going from the ESC to that motor, were swapped once the system was powered down to reverse the direction of rotation. Once the motors were tested, the stand was ready for final preparations before collecting data. The Mark 10 force sensor was connected to the monitor and powered on. The units were set to gram force and the sensor was tared. The serial monitor for the Arduino was opened and the rpm readings were checked. The battery was then connected to the y harness with the watt meter installed between the battery and the ESCs. The units on the watt meter were set to watts. At that point, the test stand was ready for data collection.

External Measurement Sensors and Parameters Tested

For the tests completed there were two external sensors used for measurements. The first was a Mark 10 force gauge. The exact gauge used was a MR03-10 which has a maximum capacity of 5000 grams of force (gF) with a resolution of 2 grams. The spec sheet for the force sensor can be found in Appendix A. The watt meter used for measuring the power input was the a Hobbyking 30A compact watt meter. The maximum ratings for this unit are 30 volts and 30 amps [11]. The manual for the watt meter can be found in Appendix A.

There were also prefabricated electrical systems not used for measurements. The first of these components were the two electronic speed controls (ESCs). These ESCs were Afro brand 30amp multi rotor ESCs. See Appendix A.4 for the data on these speed controllers. And the final prefabricated electrical system were the two brushless motors. The specific ones used were DYS Quanum MT4012 340KV motors. The only change to the motors was the use of locknuts on the propeller shaft to keep the propellers more secure during testing. The motor information can be found in Appendix A.5.

One parameter tested during the initial tests was two different propellers. The first propeller tested was a 9-inch diameter with an average pitch of 4.7 inch per revolution 2 blade propeller, 9x4.7x2. The second propeller tested had a diameter of 9 inches with an average pitch of 4.5 inch per revolution 3 blade propeller, 9x4.5x3. Another test parameter varied during the initial testing was the spacing of the

propellers. The closest spacing used was the nearest half centimeter that would allow for propeller clearance. This meant that the propeller tips were within a centimeter of each other. The furthest spacing used for the tests was twenty-one centimeters because this spacing put the motors halfway between the end of the rails and the center of the rails. And the final propeller parameter tested during the initial tests was the direction of rotation. The 9x4.5x2 propellers were tested with both propellers spinning clockwise as well as one spinning each direction.

Data Collection Methods

The parameters measured during testing were power setting in percentage, thrust in gram force, power output in watts, and rpm measurements from each motor. All the values were noted for the initial conditions, after which the motors would be started, and data points collected as the motors were incrementally increased to full power. Once at full power, the motor speed was brought down one increment and back up to full and a second set of full speed data points were gathered. After this, the motor speed setting was incrementally slowed until back to zero to ensure reversibility.

Test Data

All the raw test data may be viewed in Appendix D. The following are graphs showing the raw data from the tests. The first graphs for each propeller, Figures 6, 8, and 10, shows the thrust as a function of the rpm. The second set of graphs for each propeller, Figures 7,9, and 11, shows the thrust as a function of the power input, which shows the efficiency of the system. The single propeller tests are shown with square chart markers to help these stand out as different on the graphs.

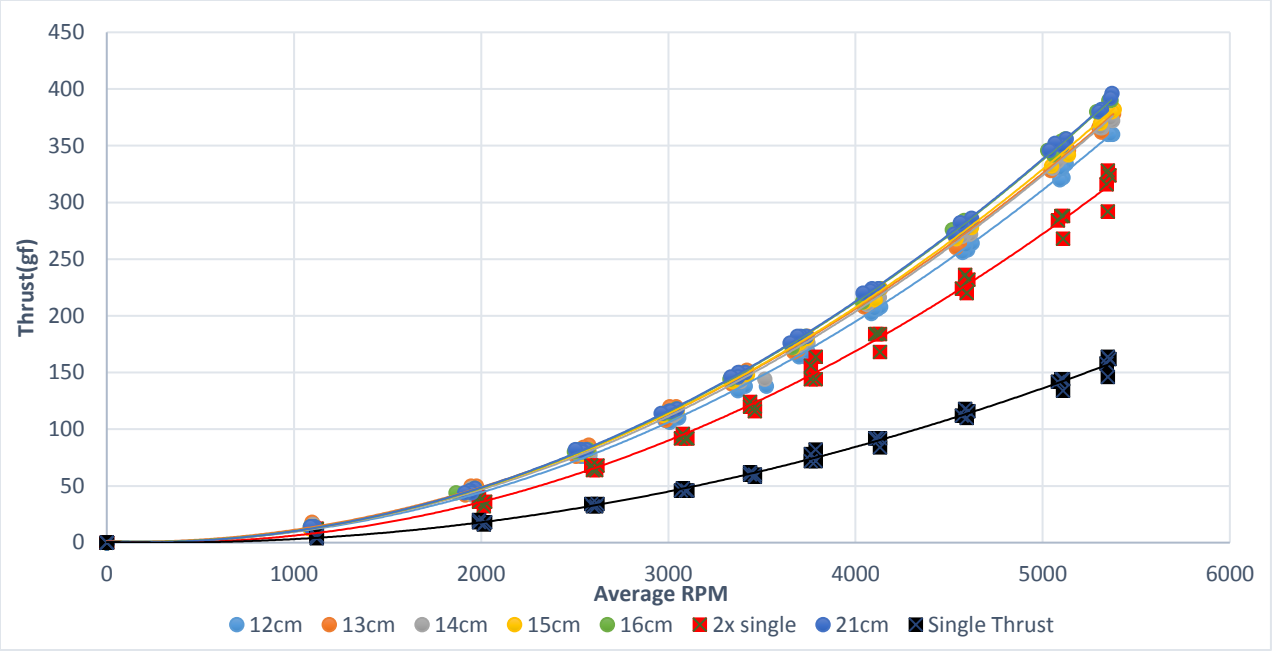

Figure 6: Scatter plot of thrust verses the average motor rpm using 9x4.7x2 propellers spinning the same direction.

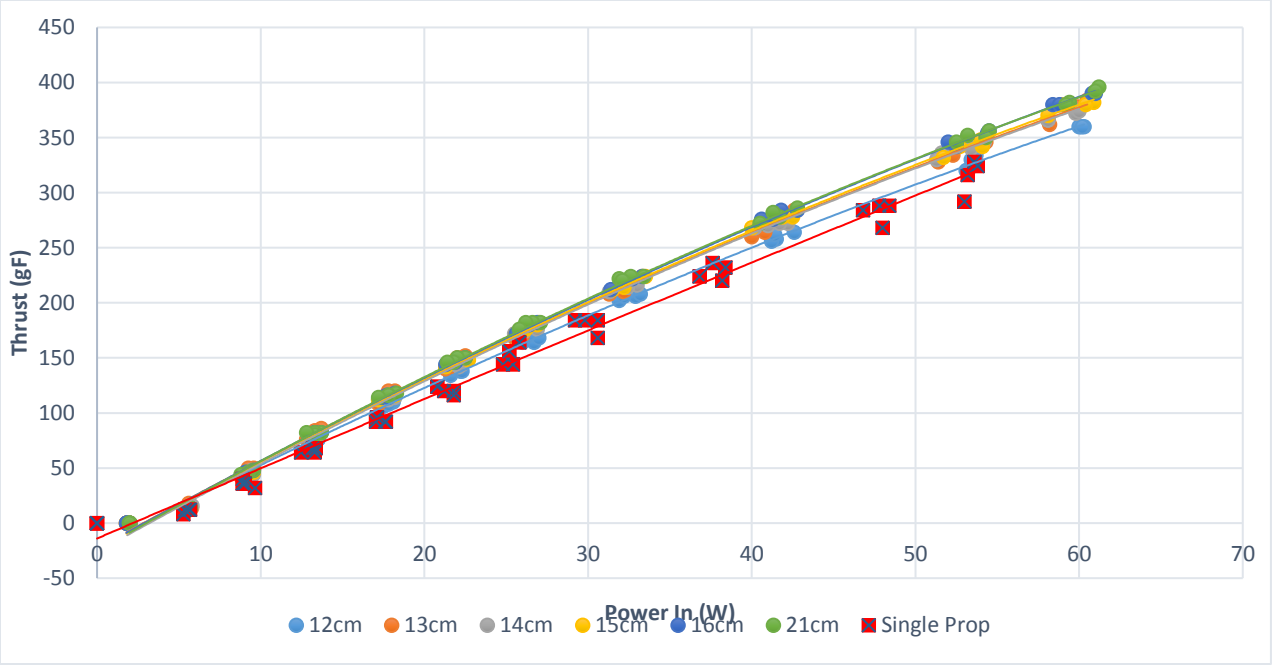

Figure 7: Scatter plot of thrust verses the total power consumed using 9x4.7x2 propellers spinning in the same direction

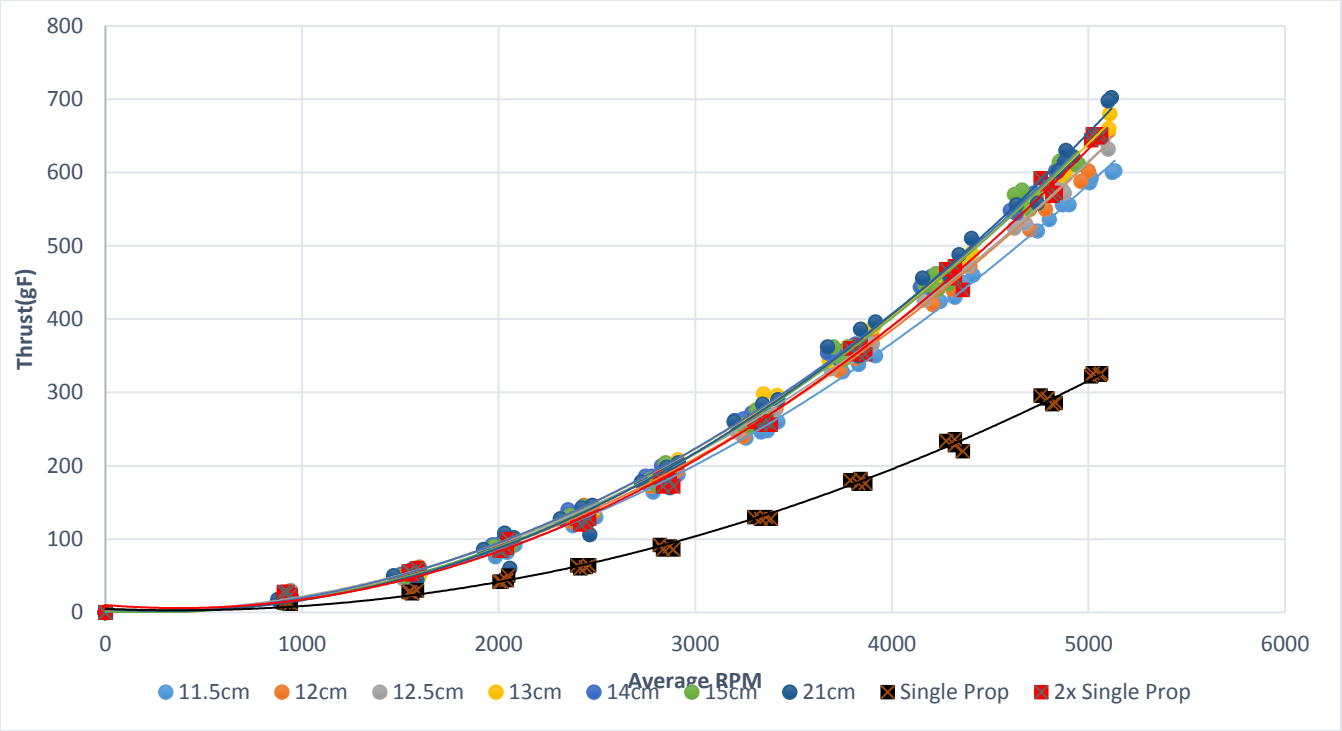

Figure 8: Scatter plot of thrust verses the average motor rpm using 9x4.5x3 propellers spinning in the same direction

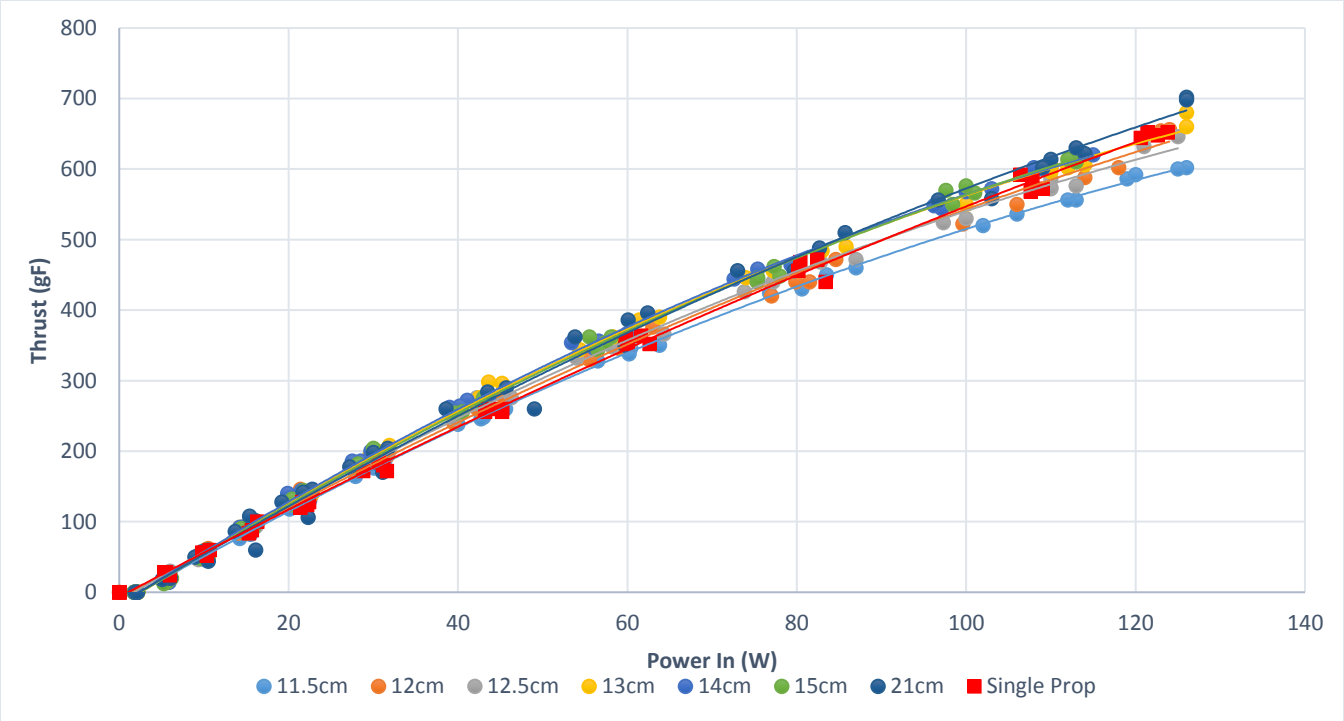

Figure 9: Scatter plot of thrust verses the total power consumed using 9x4.5x3 propellers spinning in the same direction

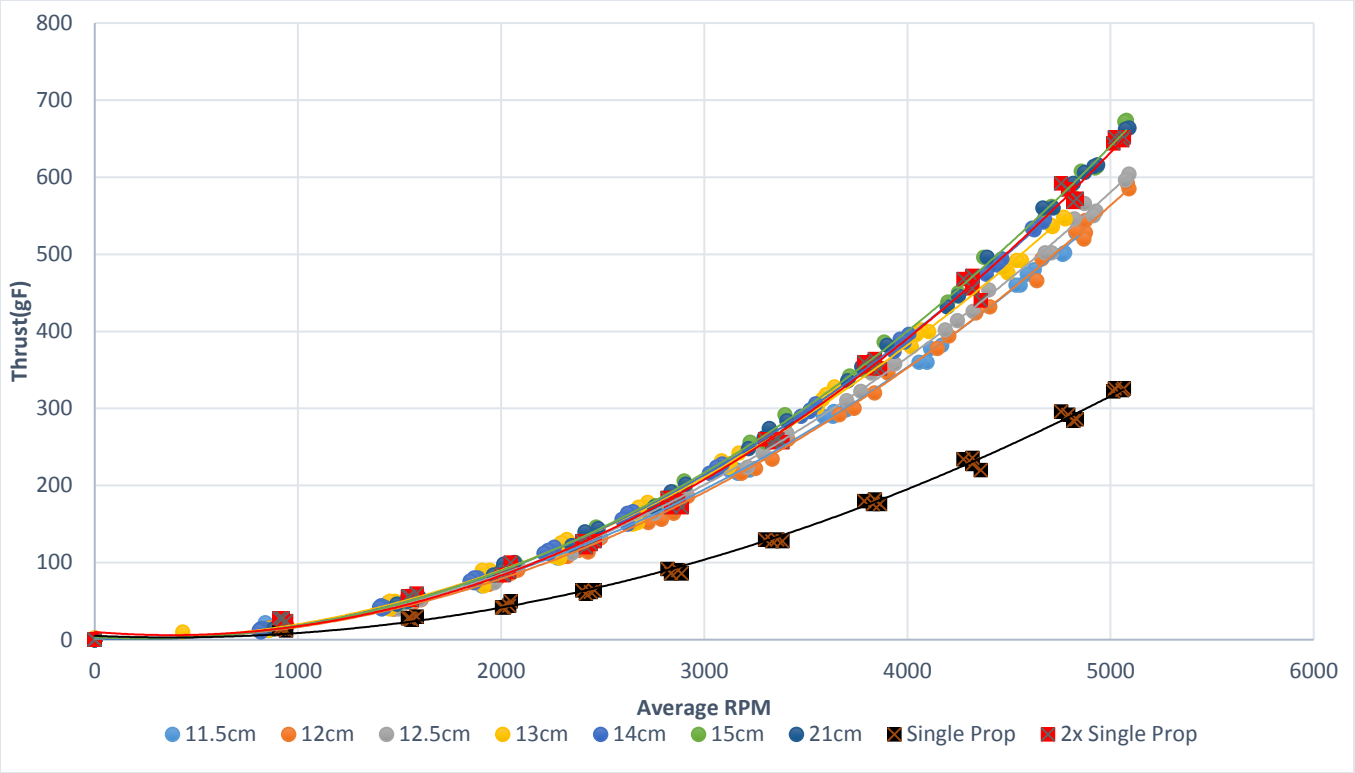

Figure 10: Scatter plot of thrust verses the average motor rpm using 9x4.5x3 propellers spinning in opposite directions

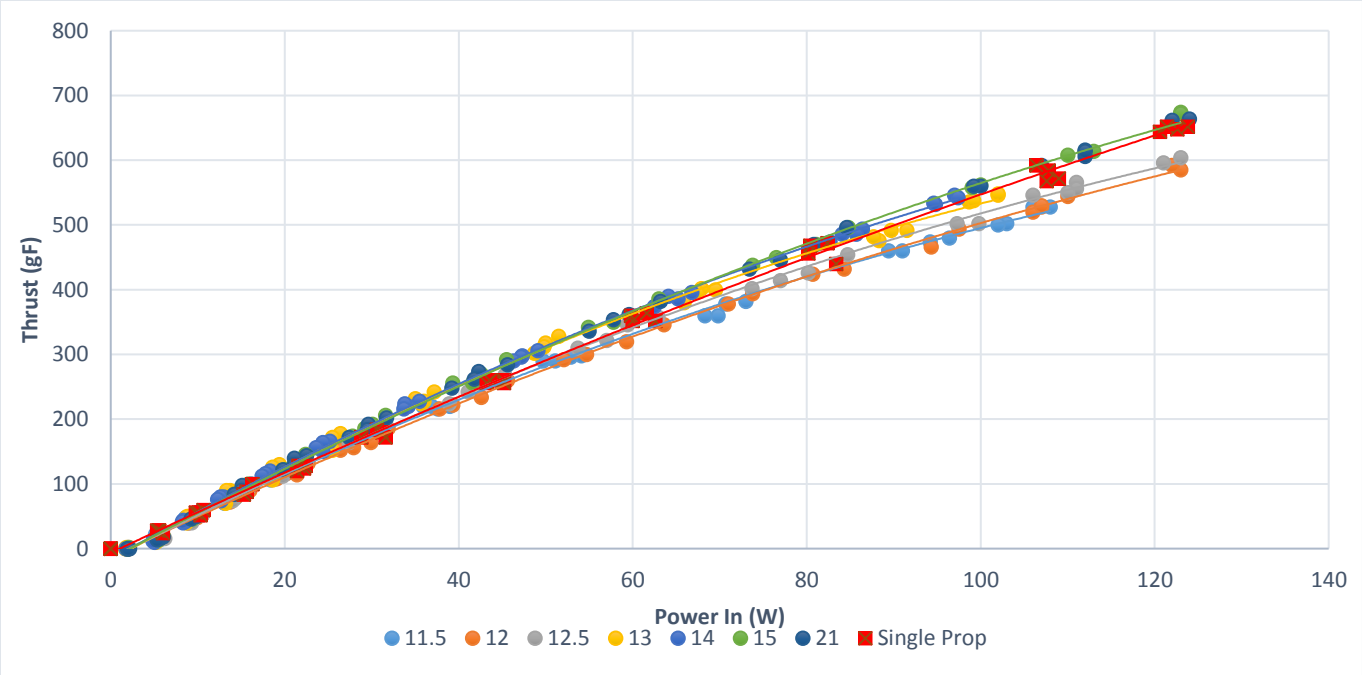

Figure 11: Scatter plot of thrust verses the total power consumed using 9x4.5x3 propellers spinning in opposite directions

Initial Data Discussion

The first trend visible in the data is that as the propellers are moved further apart, the thrust and efficiency both appear to improve. This is in line with the theory that the propellers will gain efficiency with less turbulent air. Another visible trend is that the single propeller results are inconsistent between the different propellers. In the two bladed setup, the single propeller output was much lower than the outputs from the dual propeller tests. Meanwhile, during the three-bladed test the single propeller was near the top of the outputs as expected.

Initial Analysis and Results

The first analysis done on the data was to bring the thrust verses power data into a form that matches the governing equation for static thrust. The equation for theoretical maximum static thrust can be seen in equation 1 [12].

$$P = \frac{\sqrt{\frac{1}{2*\rho*A}}}{FOM} * T^{1.5} \qquad (1)$$

In order to create a chart that fits this equation the thrust was raised to the three halves power. The data in these charts would follow a linear model with a trendline equation taking the form of y=m*x+b. The intercept value, b, would include all the inefficiencies of the system including any changes in efficiency due to synergetic efficiency. Due to the disc area (A) changing between the single and dual propeller tests, the single propeller data was not included in this comparison. The charts from these calculations can be seen in Figures 12,13, and 14.

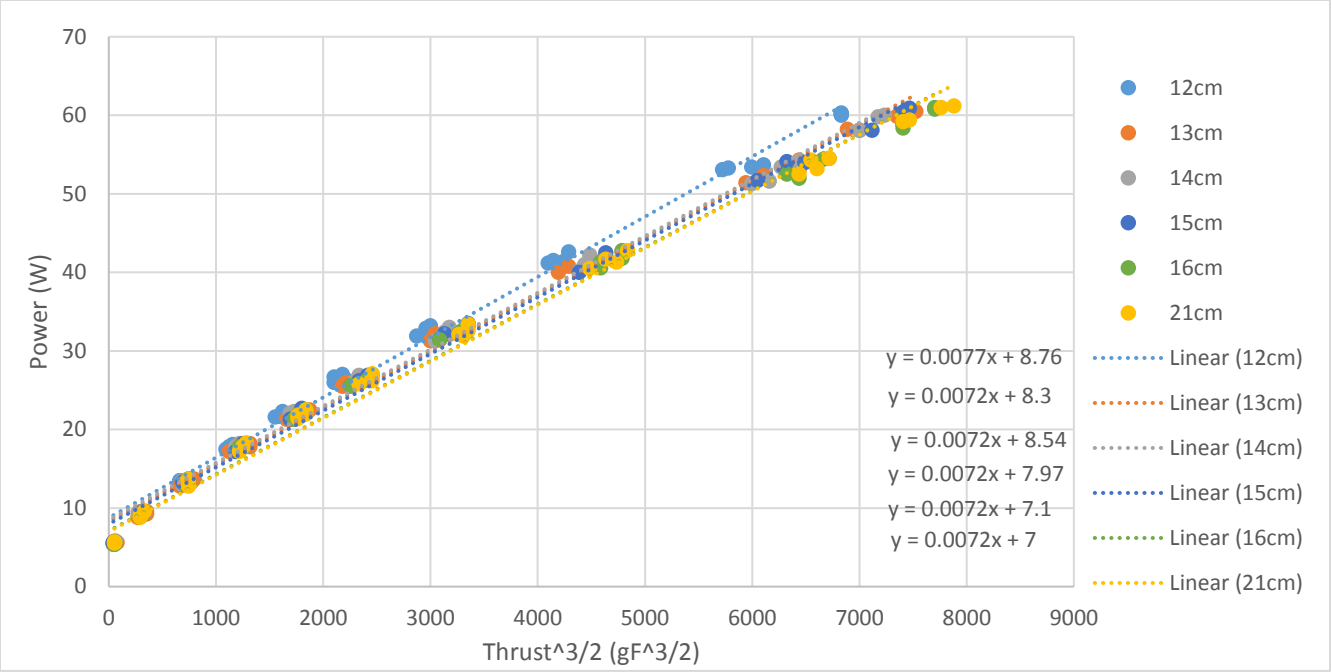

Figure 12: Scatter plot showing the power verses the thrust raised to the three halves power. Trendline equations are in the form of the governing equation for static propeller thrust.9x4.7x2 propellers spinning the same direction.

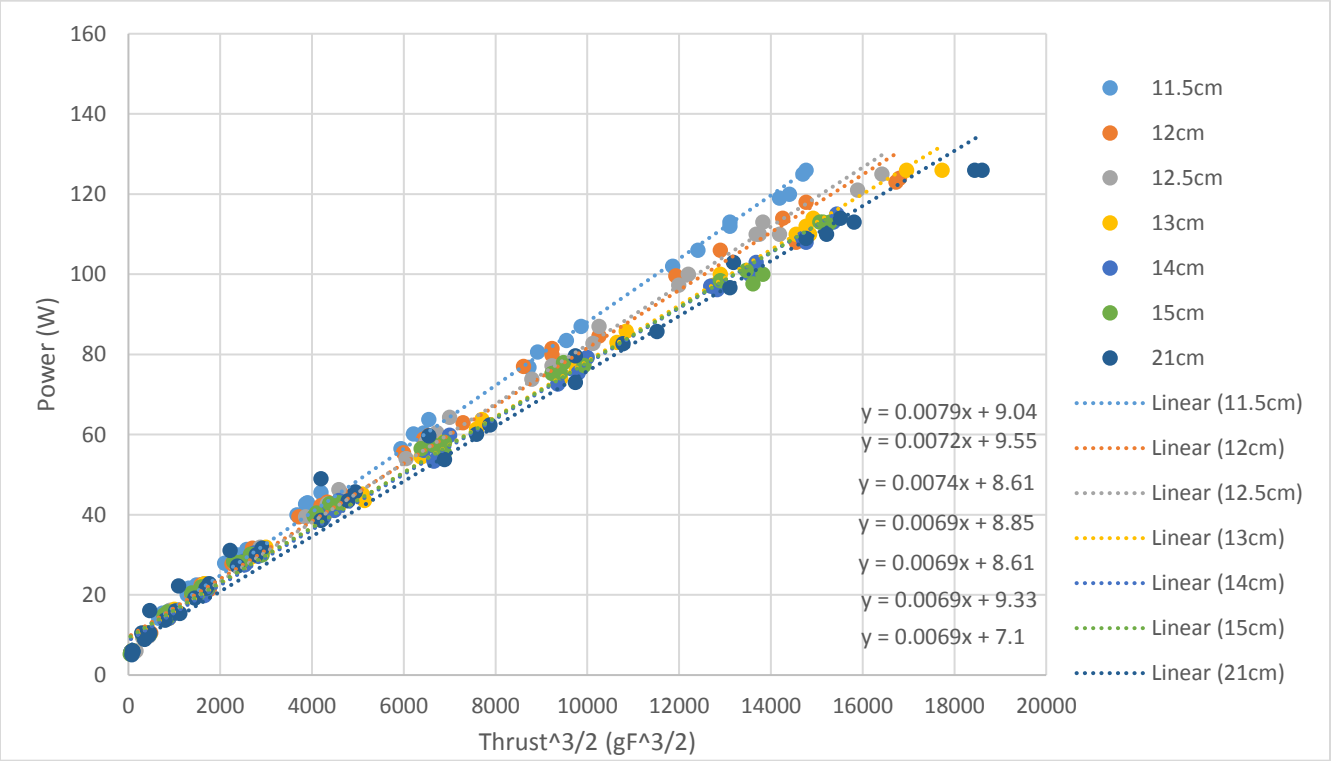

Figure 13: Scatter plot showing power verses thrust raised to the three halves power for the 9x4.5x3 propellers spinning the same direction.

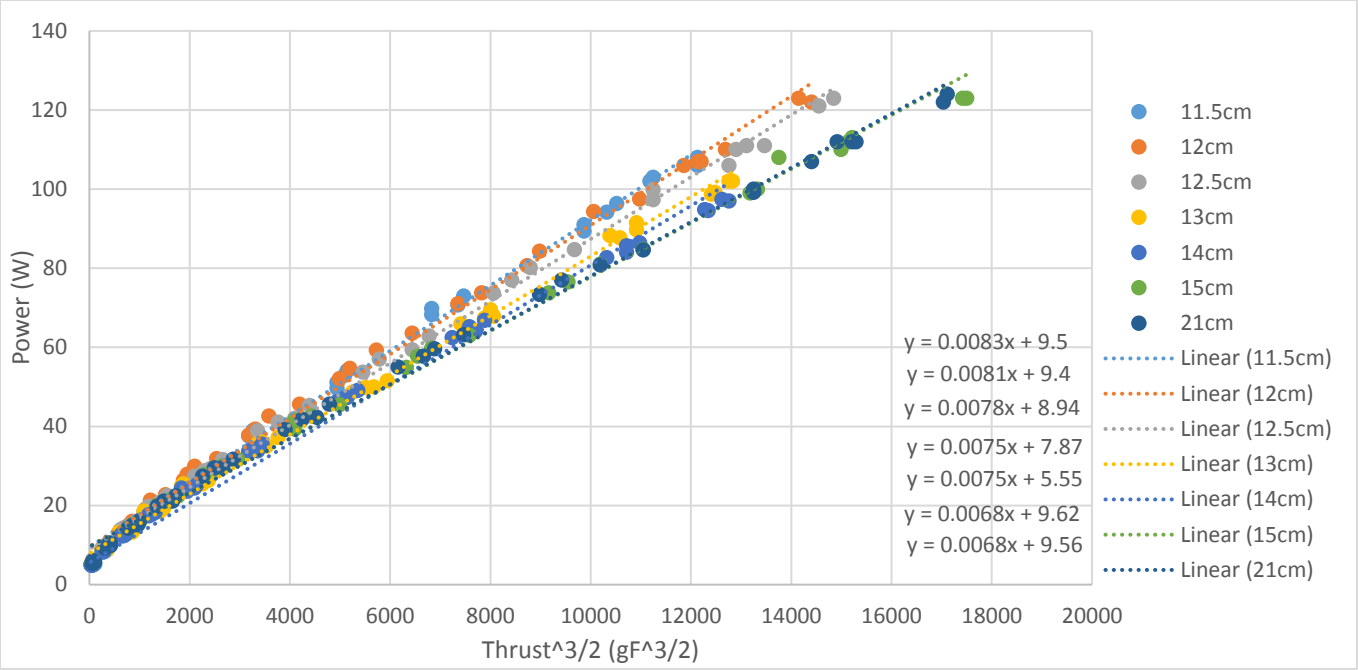

Figure 14: : Scatter plot showing power verses thrust raised to the three halves power for the 9x4.5x3 propellers spinning opposite directions.

After these charts were created the intercept values from the trendlines were used in a new graph to show how the inefficiencies, in watts(W), change with the changing motor spacing. This chart can be seen in Figure 15.

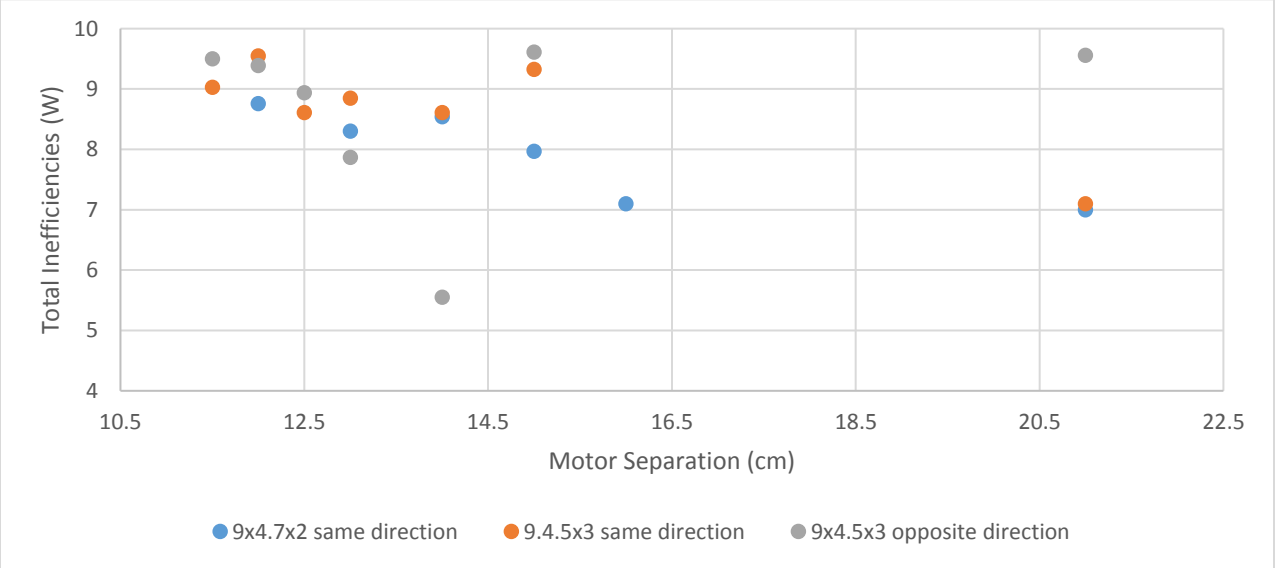

Figure 15: Scatter plot showing how the propeller systems inefficiencies change as the motor spacing is increased for all tests

Overall system efficiency was calculated by dividing the desired output (thrust) by the required input (power in) to find the grams of thrust per watt of power. This was then compared against the average rpm to make a complete motor efficiency curve for each propeller. These comparisons can be seen in Figures 16,17, and 18. This comparison is the standard used for turbomachinery systems [13]. Another calculation completed was to see how the rpm of peak efficiency changes as the motor spacing was increased. This was done by plotting the peak efficiency rpm at their designated spacing. The results from this can be seen in Figure 19.

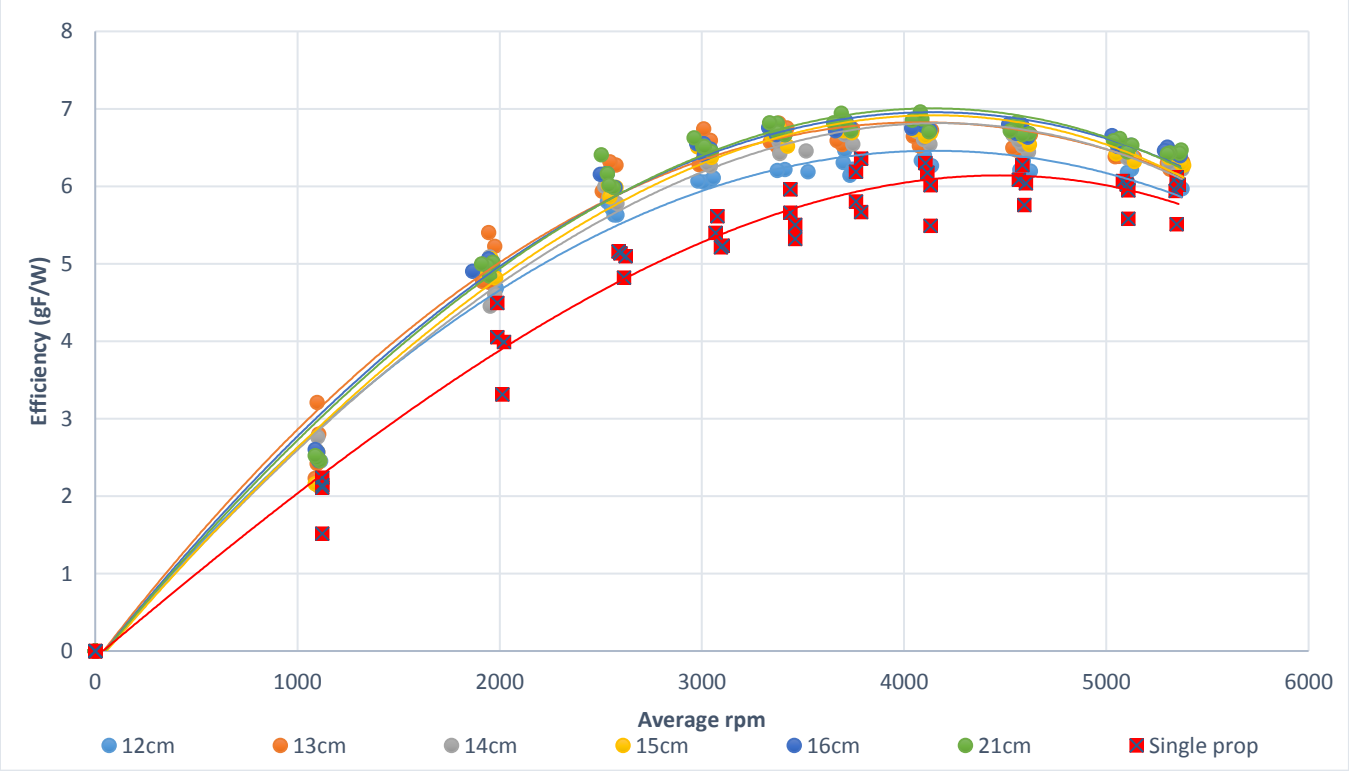

Figure 16:Scatter plot of system efficiency verses the average motor rpm for the 9x4.7x2 propellers spinning in same direction

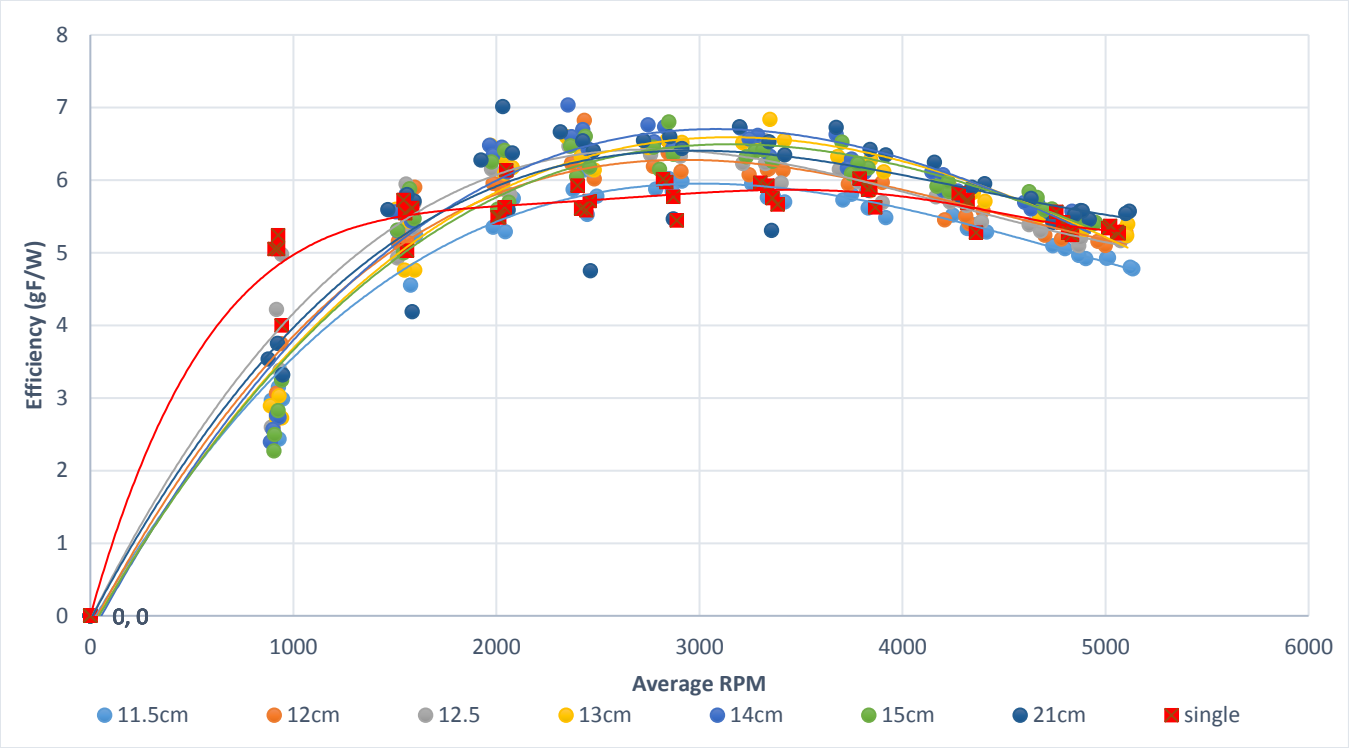

Figure 17: Efficiency vs. RPM, 9x4.5x3 propellers, same direction of rotation

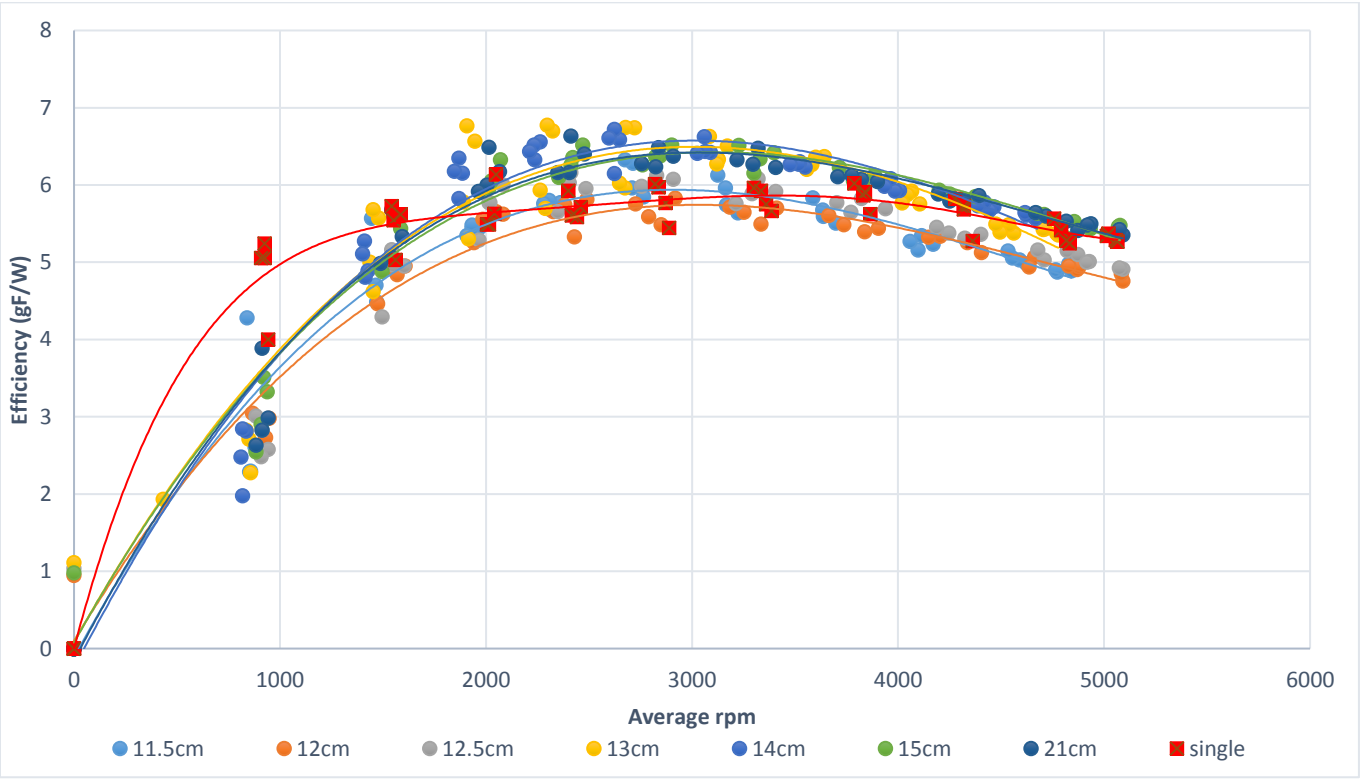

Figure 18: Efficiency vs. RPM, 9x4.5x3 propellers, opposite direction of rotation

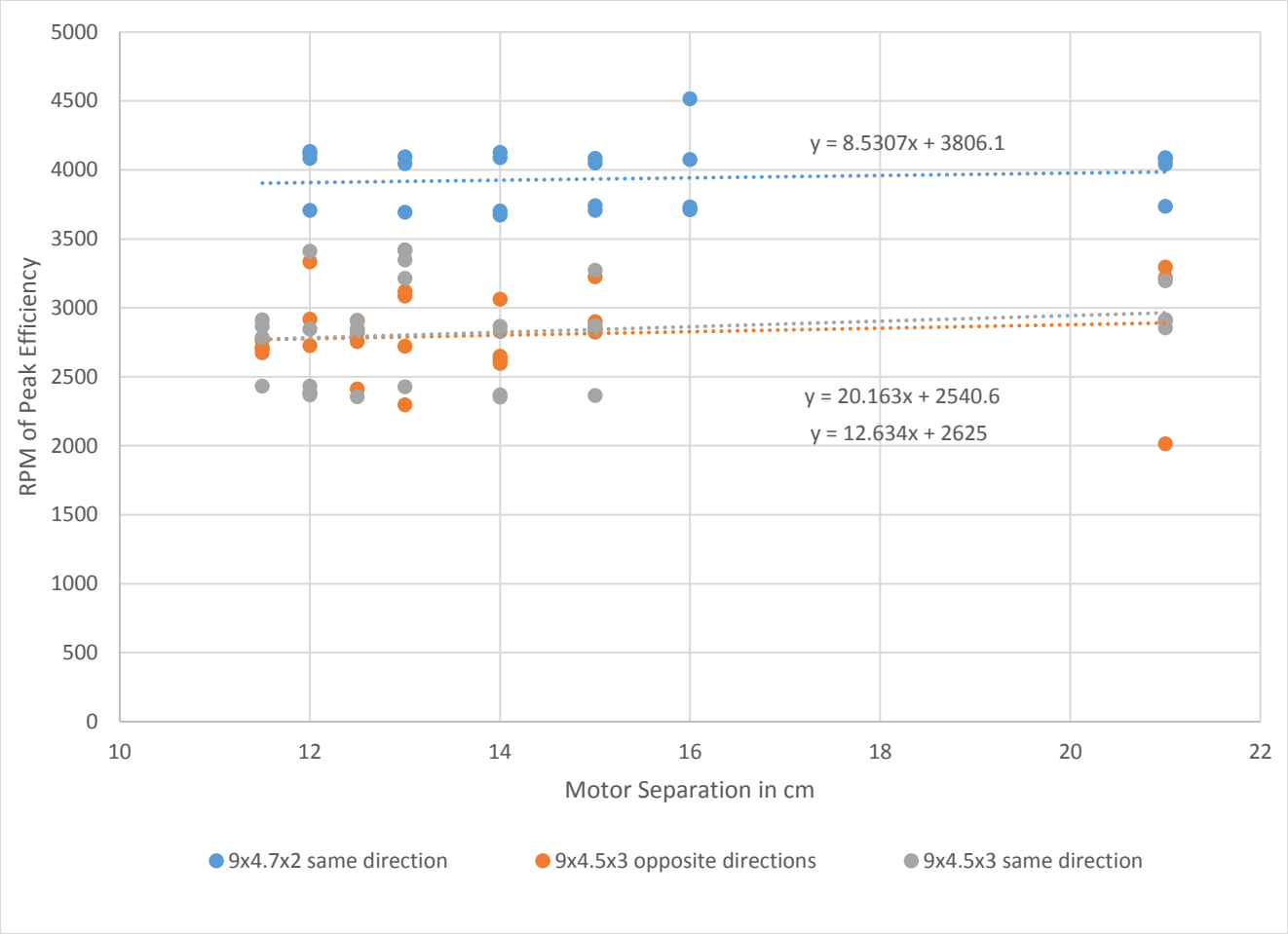

Figure 19: Scatter plot of the rpm of peak efficiency verses the motor separation for all three initial propeller tests.

Initial Analysis Discussion

The analyzed results show that as the propellers were moved further apart the efficiency went up. There was a diminishing amount of return for each centimeter of separation until the system reached the point of far field equilibrium. At that point, the data stabilized, and no major changes occurred between tests. This trend was also visible in the power verses thrust raised to the three halves power charts, Figures 12, 13, and 14. These plots show that in general as the spacing is increased the total inefficiencies goes down and the slope stays relatively constant. The inefficiencies are shown on their own in Figure 15, which shows that except for a few outlying points that the inefficiencies decrease with distance. Both results seem to show that no synergetic efficiency was gained at closer distances. Another result from the analyzed data can be seen in Figure 19. This figure shows how the peak efficiency speed

changes as the motor separation distance is increased. The slightly increasing slope of the trend shows that the speed of the peak efficiency increases slightly with the spacing. The change in rpm over the distances tested ranged from 8.53 rpm/cm to 20.16 rpm/cm.

As a final trend, it was noticed that the single prop test was not the peak efficiency as was originally expected. This could be for several reasons, but most likely is due to the change in disk area. The reason for this assumption is the non-linear relationship between power thrust, and disc area in the equation for static thrust. More testing was done to check for possible causes of this result.

Motor Height Testing

To attempt to resolve the issues with the data, a couple of different tests were done. The first test was to run a standard set of data on extension blocks to raise the motors above the rails. The main reason for doing this was to check if there was an effect from the mount in the center of the rails for the force sensor. The extension block setup may be seen in Figure 20.

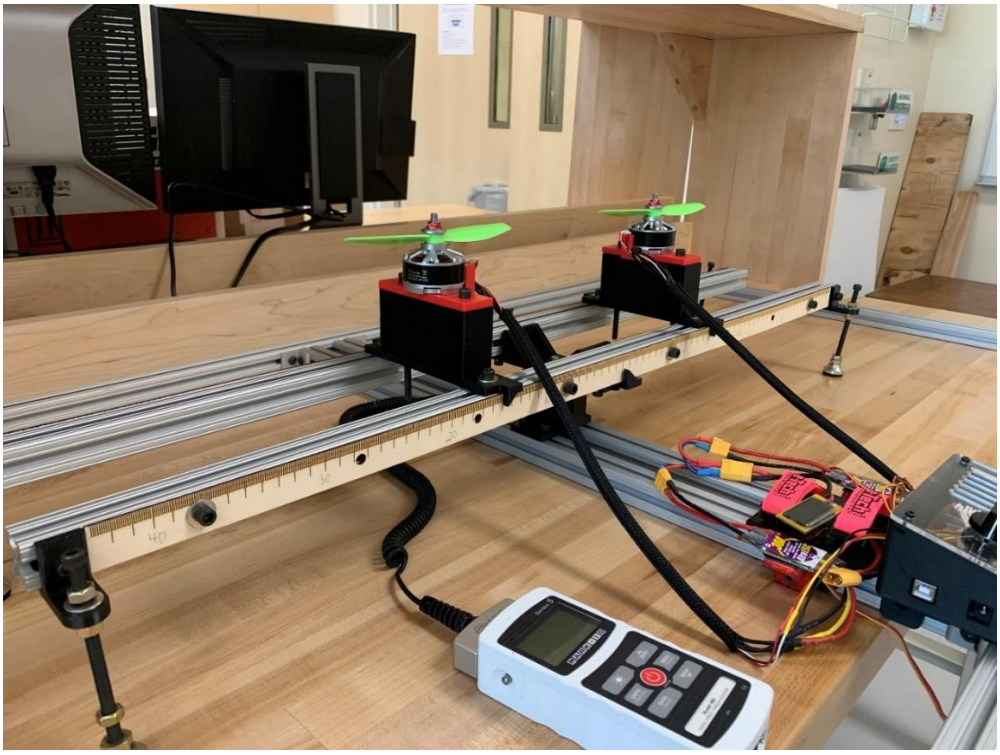

Figure 20: Motor test stand with extension blocks setup

Another purpose of this test was to show how reducing the ground effect from the rails affects the motor efficiency. This test was run using the 9x4.7x2 propellers spinning the same direction so it could be compared to earlier tests. The comparison done was the power verses thrust raised to the three halves power since it would pull the total system inefficiencies out of the data. The results of this test are below in Figures 21 and 22.

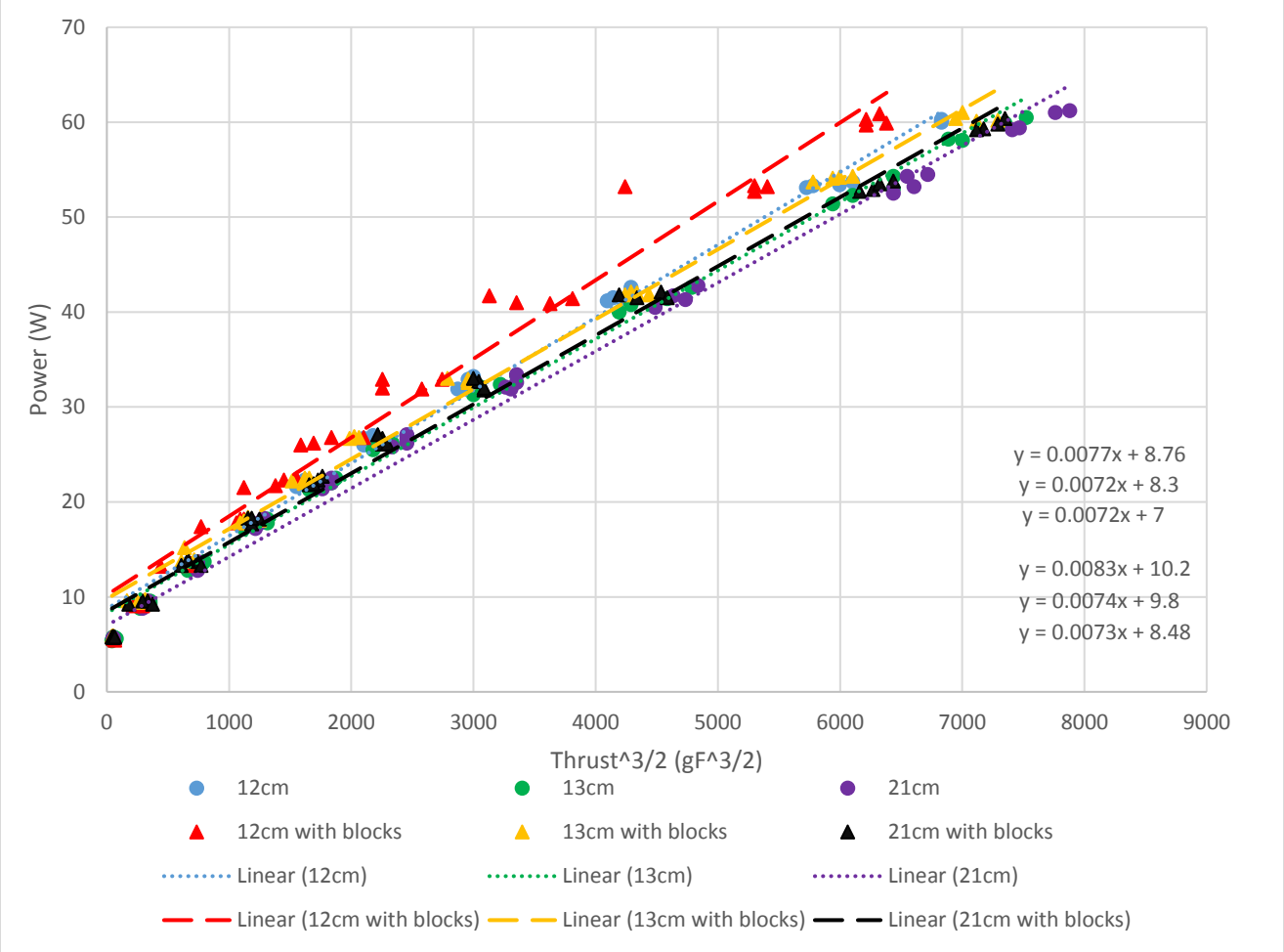

Figure 21: Scatter plot of power verses the thrust raised to the three halves power using 9x4.7x2 propellers spinning the same direction. This test was used to test the effects of different motor heights.

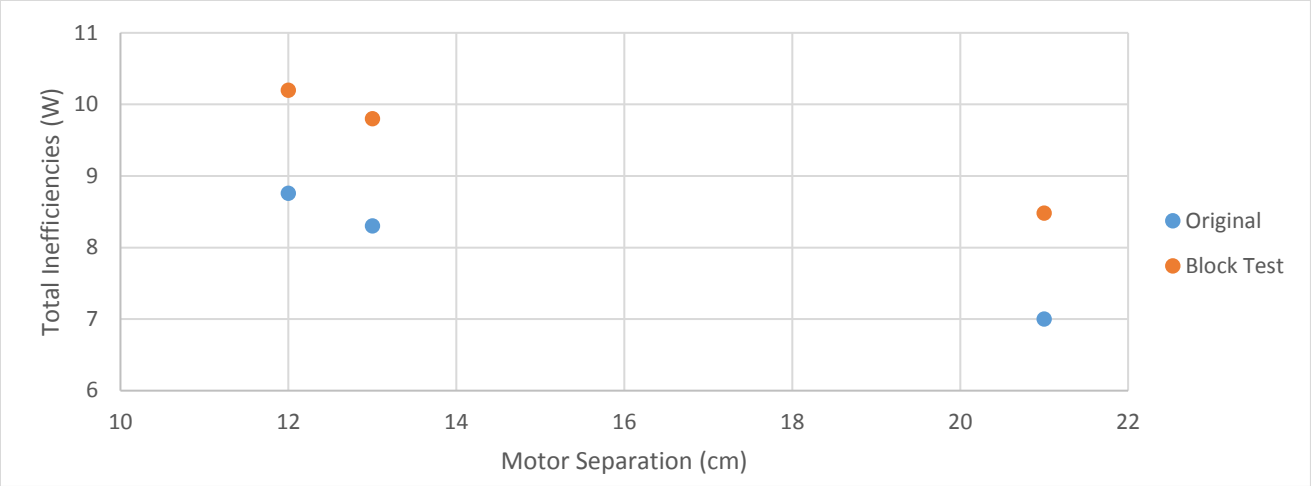

Figure 22: Scatter plot of total inefficiencies verses the motor separation for the motor height test.

Motor Height Test Discussion

The data from this test show a couple of distinctive results. The first result is that the additional frame ground effect during the lower test does improve the efficiency of the system by an average of 1.5 watts which is an increase of between 16% and 21% depending on the spacing. This was expected due to the additional efficiency airfoils gain in the ground effect region [14]. Since the inefficiencies followed a y-axis shift of 1.5 watts between the two heights tested, this led to the conclusion that the effects of center brace were minimal. This would validate the tests done at the lower height because the even though the efficiency is different, the change is a simple vertical axis shift translation.

Rail Effects Testing

The next area of retesting was designed to investigate the reasoning for the reduced efficiency of the single propeller tests. The original single motor setup may be seen in Figure 23.

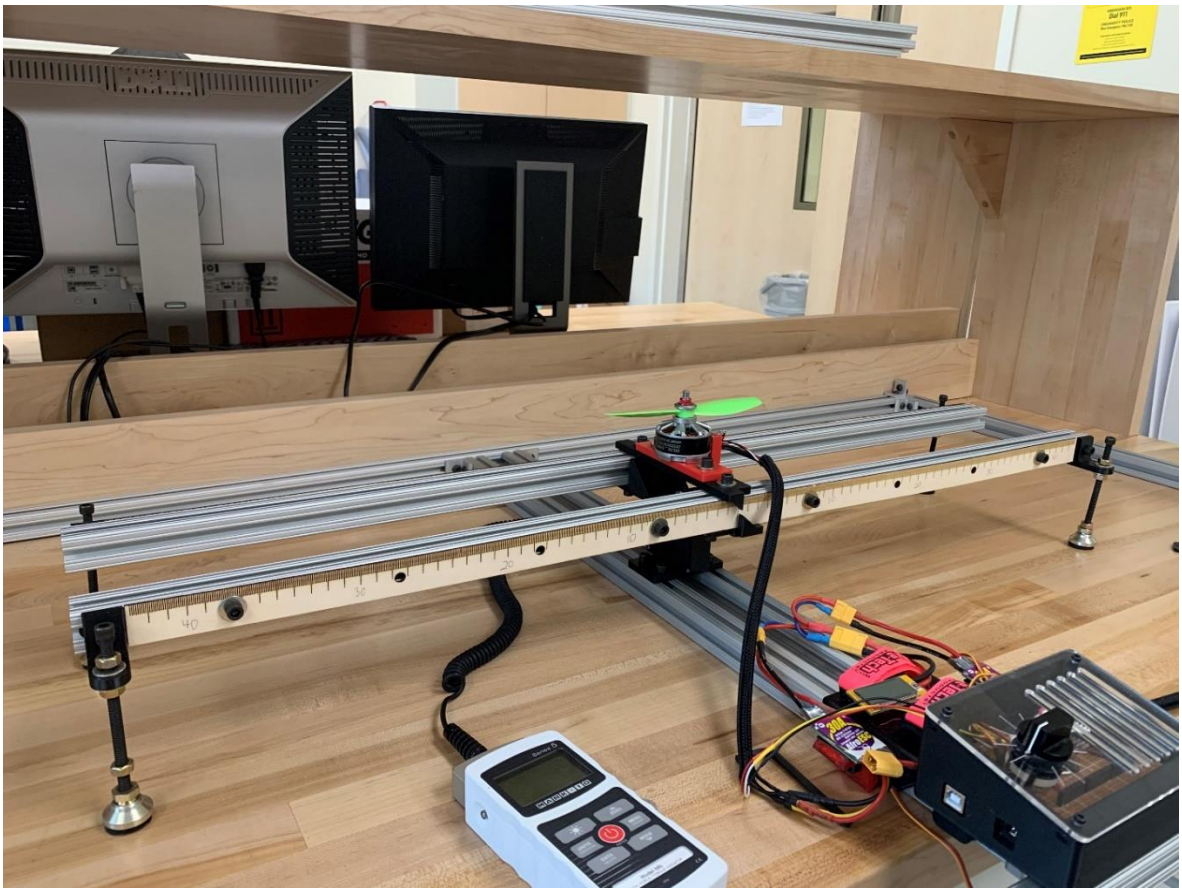

Figure 23: Original setup for single motor test

In this setup, one motor was removed, and a single motor was centered on the rail. For the new test, the rail system was removed, and a special bracket was built to mount a single motor directly to the force

sensor. This new bracket-mounting method may be seen in Figure 24.

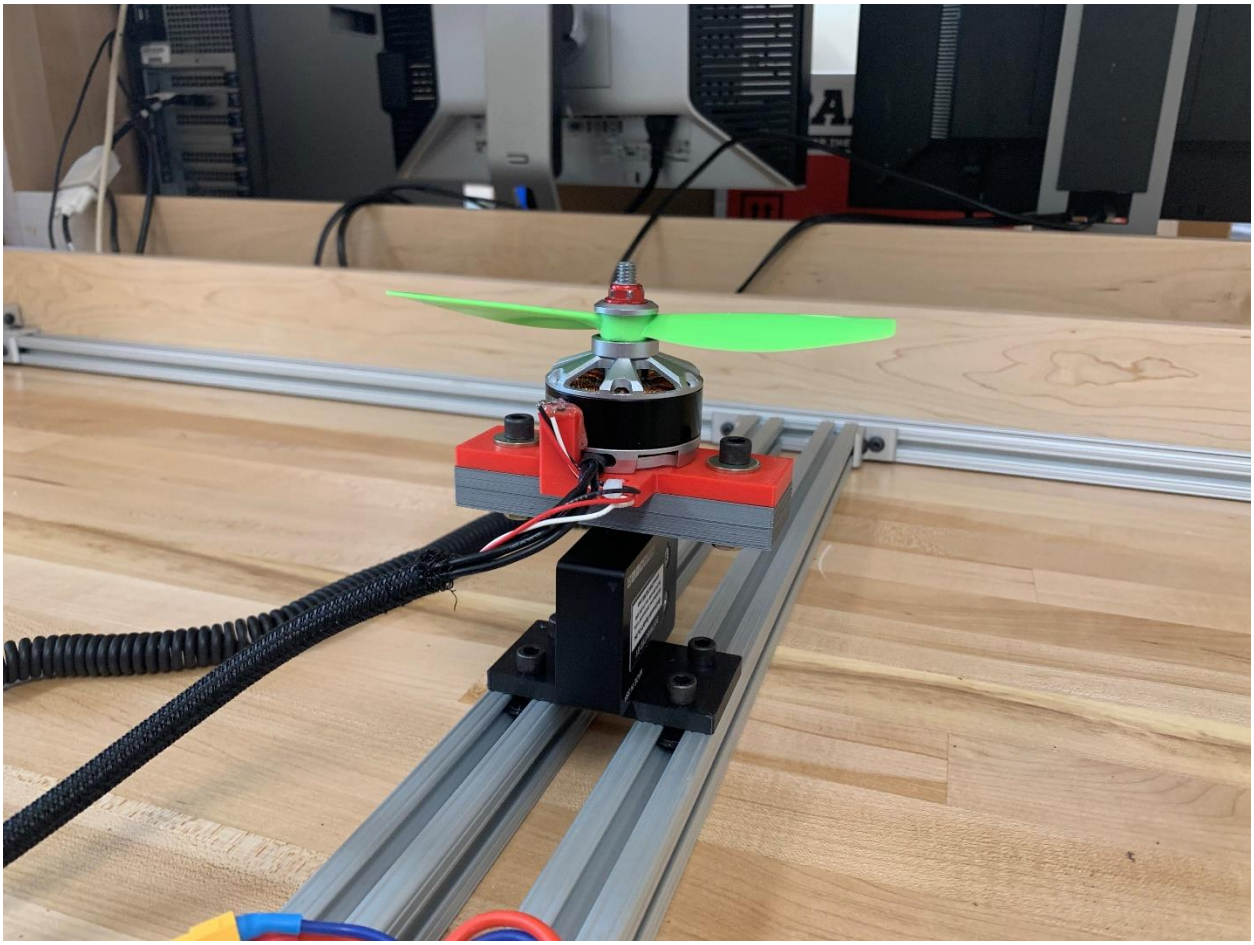

Figure 24: New single motor test setup

A data set was then created for the 9x4.5x3 propeller and compared to the results from the tests with the rails. The test result comparisons may be seen in Figures 25, 26, and 27.

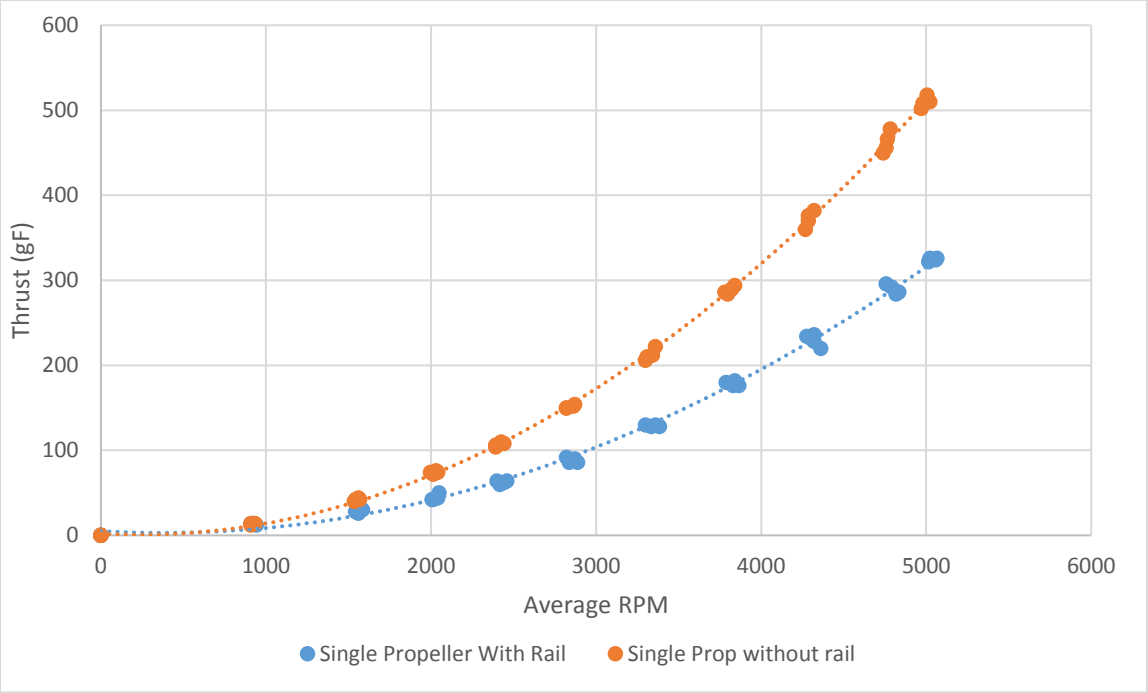

Figure 25: Scatter plot of thrust verses motor rpm comparing the two single motor setups using the 9x4.5x3 propeller

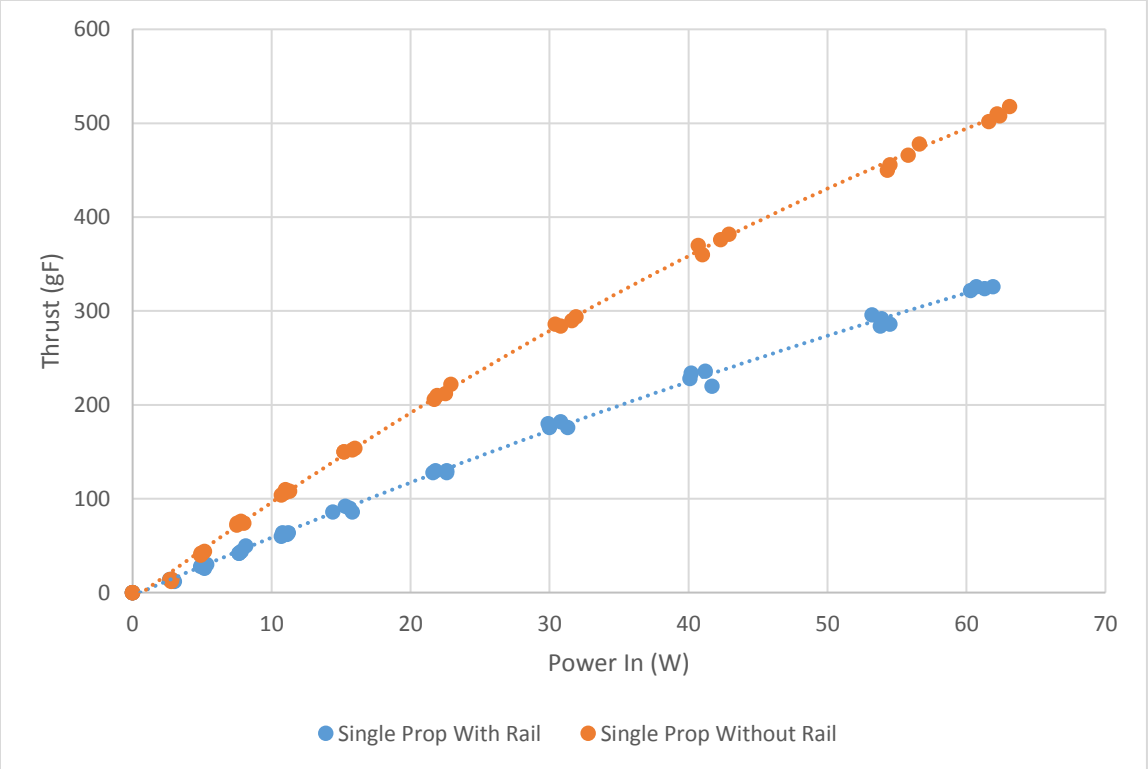

Figure 26: Scatter plot of thrust verses total power consumed comparing the two single motor setups using the 9x4.5x3 propeller

Figure 27: Scatter plot of the system efficiency verses the motor rpm. This data came from the rail effect test and was compared to the original dual motor test which used the 9x4.5x3 propellers spinning in opposite directions

Rail Effects Discussion

The results of this test show that the rails have a major influence on the performance of the motors. The average increase in efficiency without the zero conditions was 57% with a peak efficiency increase of 79%. This effect is probably due to the change in propeller disk loading. Disk loading is the weight lifted per rotor disc area of the propellers [15]. In testing of aerial systems, the hovering efficiency is negatively affected by an increase in the disk loading of a lifting propeller [15]. This would explain the efficiency losses in both comparisons. When the test stand switched from two propellers to a single

propeller lifting the rail, the disk loading of the system was doubled by reducing the area in half, by only using one propeller, while keeping the same weight. In the single propeller comparisons, the disk loading was reduced when the rail was replaced with the bracket, reducing the weight lifted by the motor. The disc loading governing equation involves the figure of merit (FOM), which is not known for the propellers tested [12]. The FOM comes from the overall efficiency of a propellers design and is found by dividing the induced velocity by the power used [12]. To find the FOM for the propellers used and confirm the disc loading theory, the test stand would need a way of measuring the induced velocity during testing. This additional data required makes this more practical for a future study. Even though disc loading cannot be numerically proven with the data gathered, the general trend of disc loading shows that is it a factor that should be accounted for in future testing [15]. Changes should be made to the test stand in order to be able to compare a single propeller to a pair of propellers as well as different sizes of propellers. The results comparing the propeller pair spacing should still be valid due to the disk loading of the propellers not changing during these tests.

Further Research

Further research is suggested in several areas. The test stand should be redesigned to minimize the effect of disk loading on the system. This would allow comparisons of single and multi-propeller systems. One possible method to do this is to use one force sensor per motor and mount each motor directly to the sensors. This would eliminate any changes in disk loading because each motor would always lift the same weight, whether one or multiple motors were running.

A round of tests is suggested to investigate the effects of running the motors at various angles instead of level. This would mimic the mounting used on multi-rotor drones to prevent turbulence during descents [16]. This angle might affect the efficiency when the propellers are closer together. The test stand could be modified to accommodate this test by modifying the black motor mounting plate to add a wedge and align the ¼-20 motor mounting bolt holes to the new angle.

A series of tests with pairs of coaxial motor systems is also recommended. These systems are starting to be used in larger multi-rotors due to their increased reliability and can be made more compact

due to using two motors on a given arm. This research could provide useful information for larger multi-rotors which are most affected by the limited flight times [1].

Conclusion

To conclude, this report led to some intriguing results. The first of these results is that the test stand design, while it does have its limits, is a capable setup for testing propeller systems. Testing showed that one of these limitations is comparing systems with different propeller disk areas, for instance different number of propellers. There are ways to redesign the stand to account for changes in disk area causing different disk loading. Even though this test stand did not allow for comparisons of different style, size, or number of propellers due to the disk loading affect, the system was used to gather useful data. The first area of useful data gathered was the comparison of two identical propellers as the spacing was increased. This data was able to point towards the general trend of that for dual propeller systems that the efficiency increases with the propeller spacing until the efficiency reaches that of the far field propellers. At that point, the system does not gain any more efficiency with distance. Another finding was that the direction of the propellers in relation to each other did not influence this trend. All these findings would benefit from further studies in order to better focus on trends and remove outliers. Further research could also be done in several other areas, including different types of propeller, angled motors, and the effects of external airflow. So overall, this study resulted in a test stand and fundamental data which would provide a good foundation for a future research study.

References

[1] Plaza, Juan “How Will Extended Flight Time for Drones be Powered?,” Commercial UAV News website, May 20, 2019, https://www.commercialuavnews.com/infrastructure/extended-flight-time-for-drones.

[2] Diversified Communications, 2018, ”Energy Industry Executive Roundtable Report-Challenges and experiences in the use of UAVs in the energy industry,” Commercial UAV News.

[3] Hezaveh, S.H., Bou-Zeid, E., Dabiri, J., Kinzel, M., Cortina, G., and Martinelli, L., 2018, ”Increasing the Power Production of Vertical-Axis Wind-Turbine Farms Using Synergistic Clustering,” Boundary-Layer Meteorology, **169**(2), pp. 275-296.

[4] Wang, K., Zhou, Z., Zhu, X., and Xu, X., 2018, “Aerodynamic design of multi-propeller/wing integration at low Reynolds numbers,” Aerospace Science and Technology, **84**, pp.1-17.

[5] “PID Theory Explained,” last modified March 17, 2020, accessed April 17, 2020, https://www.ni.com/en-us/innovations/white-papers/06/pid-theory-explained.html.

[6] “Button,” last modified July 7, 2015, accessed April 17, 2020, https://www.arduino.cc/en/tutorial/button.

[7] “Servo Library,” last modified December 24, 2019, accessed April 17, 2020, https://www.arduino.cc/en/reference/servo.

[8] Sanjeev, Arvind “Use a Hall effect sensor to detect the presence of a magnet and make a speedometer, a burglar alarm, and more!,” Maker Pro website, March 23, 2018

[9] “writeMicroseconds(),” accessed April 17, 2020, https://www.arduino.cc/en/Reference/ServoWriteMicroseconds.

[10] “Timer1,” last modified October 2009, accessed April 17, 2020, https://playground.arduino.cc/Code/Timer1/.

[11] “HobbyKing Compact 30A Watt Meter and Power Analyzer,” accessed June 1, 2020, https://hobbyking.com/en_us/hobbykingr-compact-30a-watt-meter-and-power-analyzer.html

[12] “Theoretical Max Propeller Efficiency,” accessed May 23,2020, https://www.jefflewis.net/aviation_theory-theo_prop_eff.html.

[13] Peng, W. W., 2008, *Fundamentals of Turbomachinery*, John Wiley & Sons, Inc., Hoboken, NJ.

[14] Betz, A., 1937, “The Ground Effect on Lifting Propellers,” No. 836, National Advisory Committee for Aeronautics, Washington D.C.

[15] “Disc Loading and Hover Efficiency,” accessed April 17, 2020, https://www.krossblade.com/disc-loading-and-hover-efficiency.

[16] Chen, Z. J., K. A. Stol, and Richards, P. J., 2019 "Preliminary Design of Multirotor UAVs with Tilted-Rotors for Improved Disturbance Rejection Capability." Aerospace Science and Technology, **92**, pp. 635-643

Appendix A

Specification Sheets for Test Stand Systems

See attached files for the following appendices

A.1 Hall Effect Sensor Data Sheet

A.2 Mark 10 Force Sensor Data Sheet

A.3 Watt Meter Manual

A.4 Product Information Page for Electronic Speed Controllers

A.5 Product Information Page for Motors

Appendix B

Complete Electronic Circuit Diagram

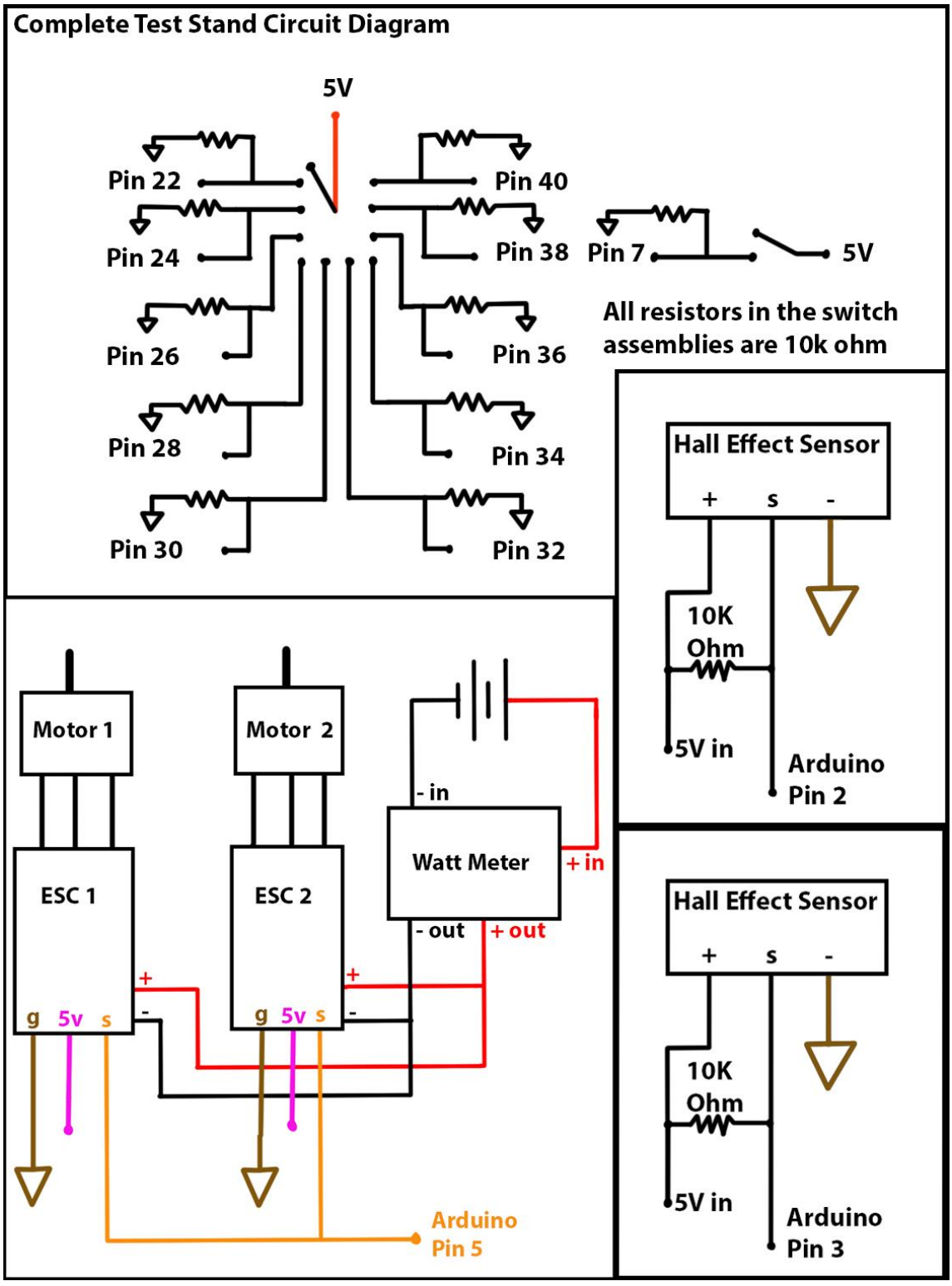

Appendix C

Arduino Code

See attached files for Arduino code

Appendix D

Raw Test Data

See the attached files for the raw data